Pion-nucleon partial-wave analysis to 1100 MeV

Richard A. Arndt, John M. Ford,* and L. David Roper
Department of Physics, Virginia Polytechnic Institute and State University, Blacksburg, Virginia
(Received 24 January 1985)

Comprehensive analyses of pion-nucleon elastic scattering data below 1100-MeV laboratory kinetic energy are presented. The data base from which an energy-dependent solution and 23 single-energy solutions are obtained consists of 3771 π^+p elastic, 4942 π^-p elastic, and 717 π^-p charge-exchange data. Partial-wave structure is characterized by the location in the complex energy plane of dominant poles and zeros, which are related to π-N resonances. Scattering lengths are extracted from the energy-dependent solution to characterize the low-energy behavior. We describe a method for charge-correcting "nuclear" amplitudes in order to use them in various charge channels; the resultant splitting between π^+p and π^-p channels is necessary and sufficient to describe the data accurately. Comparison to the Karlsruhe-Helsinki analyses is favorable, although some small differences exist. We describe how the full data base and solution files can be accessed through our scattering analysis interactive dial-in (SAID) computer system at VPI&SU, copies of which also exist at several institutions throughout the world and which can be transferred to any site with a VAX/VMS computer system. In addition to solutions presented here, SAID also encodes the Karlsruhe-Helsinki solution, the Carnegie-Mellon—Berkeley solution, and production partial waves from a recent VPI&SU analysis. The system can be used to modify solutions, plan experiments, and obtain any of the multitude of predictions which derive from partial-wave analyses of the world data base.

I. INTRODUCTION

We have updated our pion-nucleon partial-wave analysis in the first two resonance regions (up to 1100-MeV laboratory kinetic energy). All of the data and our partial-wave amplitudes are available in great detail on our scattering analysis interactive dial-in (SAID) computer system (see below), which is available at about forty other sites with VAX/VMS computers. This is a report of our energy-dependent and single-energy solutions.

Section II contains a description of the data base used to extract the solutions reported in this paper. Section III describes the parametrization of the energy-dependent solution and Sec. IV describes our method of binning the data and using partial-wave energy derivatives in order to perform 23 single-energy analyses. Section V describes our method for charge-correcting "nuclear" partial waves for use in constructing charge-channel amplitudes; we indicate how the data demand such splitting and how our method appears sufficient to satisfy the data. Section VI reports the scattering lengths extracted from the energy-dependent analysis, and indicates the range of validity for such a low-energy representation. In Sec. VII we report results for the 24 analyses of this paper, and characterize the dominant energy-dependent features of our solutions in terms of the positions of nearby complex-plane poles and zeros of the partial-wave amplitudes. In Sec. VIII we compare the features of our solutions to those of the Karlsruhe-Helsinki solution.[1] Section IX describes how the SAID facility can be used to explore π-N scattering with several solutions and the data base.

II. PION-NUCLEON DATA BASE

We have attempted to indicate the dimensions of the data base used for these analyses in Fig. 1 where we present kinematic distribution plots for cross sections and polarization measurements in the three charge channels π^+p, π^-p, and π^-p charge exchange (CXS). Each data point is indicated in Fig. 1 as "old" (boxes, before 1975), or "new" (N, after 1974). Figure 2 shows total cross sections, while Fig. 3 shows the real part of the non-spin-flip amplitude [Re$f(0)$] for π^+p and π^-p data. Because of the very large number of experiments involved, we make no attempt to detail the data base here. In compiling the data base shown in Figs. 1—3, we have excluded some very old data having large errors (e.g., polarization measurements with errors larger than 0.2), and some total-cross-section data which were incompatible with the bulk of recent, precise measurements; the deleted total cross sections are shown in Fig. 2 with a slanted line drawn through them.

We believe that our data base is the most comprehensive collection of both published and unpublished (but "respectable") data below $T_{\rm lab}=1200$ MeV. A detailed examination of the data base is possible through the SAID facility, where references and remarks are encoded. Experiments or single data points which were not included in these analyses are plainly flagged by the SAID programs.

It is important to recognize that, as revealed by Figs. 1—3, the data base used for these analyses is very large and inclusive. Inclusion or omission of single data points, or of selected experiments should not have a large effect

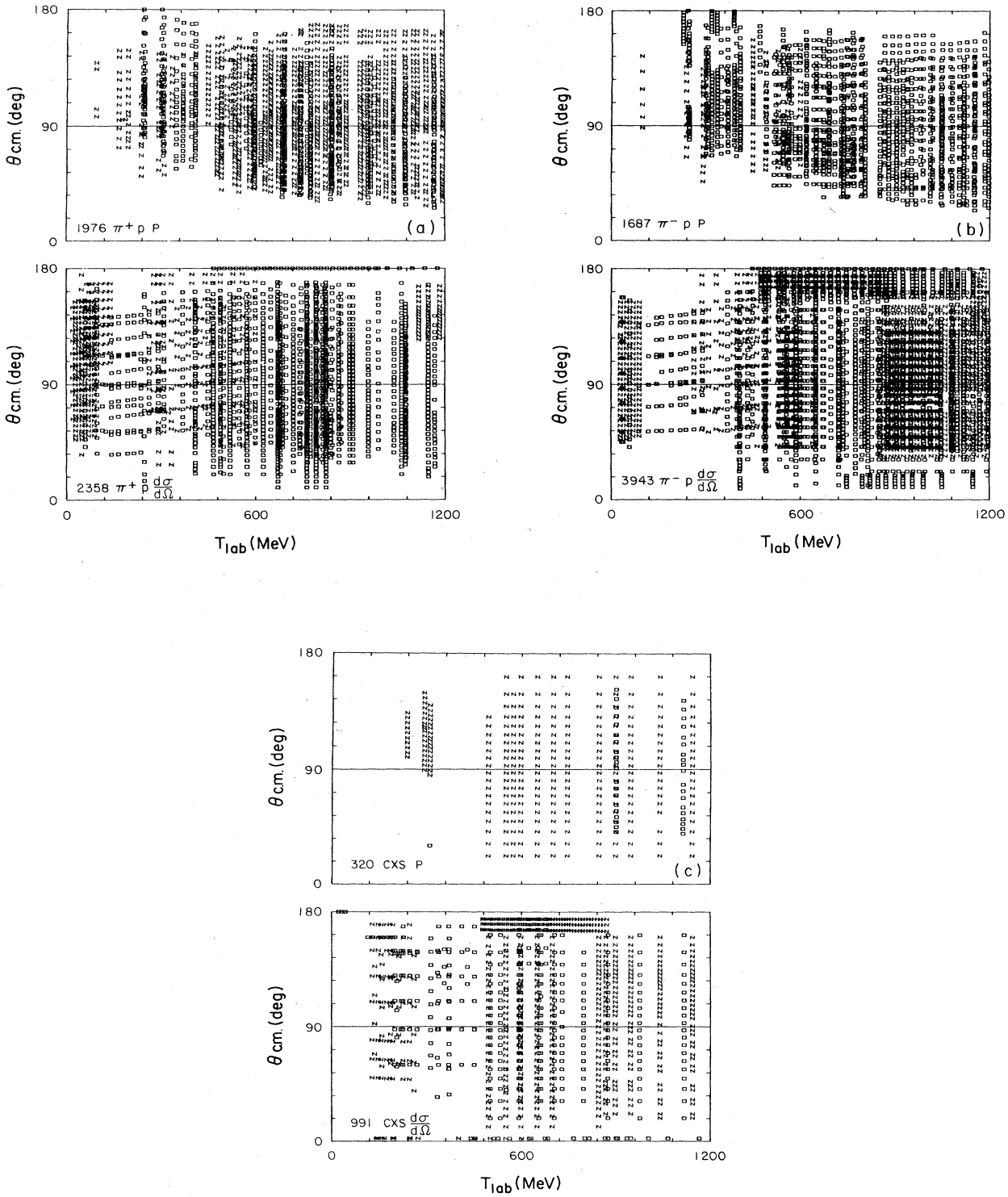

FIG. 1. Pion-nucleon scattering data base for 0—1100 laboratory kinetic energy. These graphs indicate the density and distribution of data with energy and c.m. scattering angle. The boxes indicate old data (pre 1975) and the N's indicate new data (post 1974). (a) Differential cross section and polarization for π^+p scattering. (b) Differential cross section and polarization for π^-p scattering. (c) Differential cross section and polarization for CXS scattering.

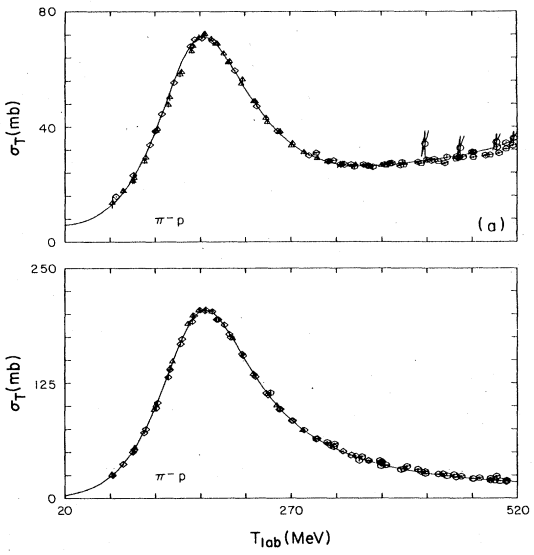

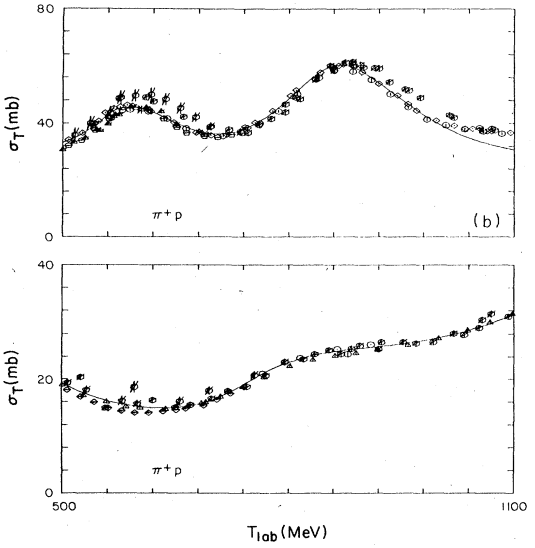

FIG. 2. Total cross section. A slash through a data point indicates that it was not used in these analyses. Curves are predictions for solution FP84. (a) Total cross section for π^+p and π^-p scattering for $T_{\rm lab}=20-520$ MeV. (b) Total cross section for π^+p and π^-p scattering for $T_{\rm lab}=500-1100$ MeV.

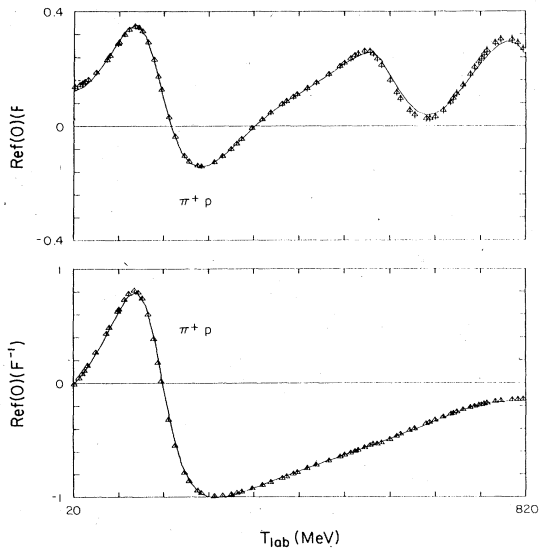

FIG. 3. Real part of the forward non-spin-flip amplitude, Re$f(0)$. Data points are dispersion-theory calculations by Carter *et al.* (Ref. 4). Curves are predictions of solution FP84.

on the solutions we obtain; in fact, we find that this is the case.

III. PARAMETRIZATION OF THE ENERGY-DEPENDENT SOLUTION

Our energy-dependent solution, FP84, is parametrized by a Chew-Mandelstam coupled-channel K-matrix form:

$$T_n=[\rho^{1/2}K(1-CK)^{-1}\rho^{1/2}]_{11}\ , \tag{1}$$

where T_n is the elastic nuclear T-matrix element, K is a real symmetric 2×2 matrix, and C is a 2×2 diagonal matrix whose elements are obtained by integrating phase-space factors over appropriate unitarity cuts. Note that $\rho=\mathrm{Im}C$ is the phase-space factor. We chose C to be

$$C_l=\int_0^1[x^{l+1/2}/(x-z)]dx/\pi\ , \tag{2}$$

where

$z=(W-W_t)/(W-W_z)$,

W = center-of-mass energy ,

l = orbital angular momentum index ,

W_t = threshold energy

$=M+\mu$ for the elastic channel

$=M_\Delta+\mu$ for the inelastic channel ,

W_z = subtraction point

$=M+\mu-150$ MeV for the elastic channel

$=M+2\mu$ for the inelastic channel ,

M = nucleon mass, μ = pion mass ,

and

$M_\Delta=\Delta$ mass .

We chose as the inelastic channel the lowest orbital $\pi\Delta$ state to which an elastic π^-p partial wave can couple. An exception is the S_{11} state, which includes coupling to a second inelastic S-wave η production channel; this can be seen clearly in the S_{11} amplitudes of Fig. 6(a).

The elastic T matrix given above satisfies elastic unitarity requirements above pion production, about 200-MeV

laboratory kinetic energy. Below threshold, a negative phase-space factor for the inelastic reaction can produce small violations of unitarity. We correct this problem to ensure elastic unitarity below 200 MeV by using the real part of the effective K matrix,

$$K_{\text{eff}}=\text{Re}[T_n/(1+iT_n)] , \tag{3}$$

to generate an elastic, unitary T matrix:

$$T_{\text{elastic}}=K_{\text{eff}}/(1-iK_{\text{eff}}) . \tag{4}$$

The K-matrix elements are parametrized as polynomials in the barycentric energy W and may also contain explicit pole terms. This apparently is flexible enough to encode all observed energy structures while maintaining proper analyticity and unitarity requirements. A high degree of smoothing occurs, as indicated in Fig. 6.

IV. BINNING THE DATA: SINGLE-ENERGY ANALYSES

Data were binned at 23 energies from 30 to 1100 MeV where "single-energy" or "energy-band" analyses were performed. The data base was first pruned with solution FP84, as described in Sec. VII, and linearized partial-wave parameters D and R were obtained. These parameters are related to the partial-wave S matrix by

$$S_l=(\cos R)e^{2iD} . \tag{5}$$

We then represent them at the analysis energy T_0 by

$$\begin{aligned} D&=D_0+D_p(T-T_0) , \\ R&=R_0+R_p(T-T_0) . \end{aligned} \tag{6}$$

The parameters D, R, D_p, and R_p were extracted from solution FP84 at the analysis energy T_0. The parameters D_0 and R_0 were varied while the parameters D_p and R_p were held fixed at their FP84 values at each single-energy-analysis energy. The number of searched parameters ranged from 4 at 30 MeV to 35 at 1100 MeV. Note that the unsearched parameters for all partial waves were fixed at their FP84 values and not set to zero; in effect giving us a "modified energy-band" analysis, in which l values higher than usual are used at each energy. That is, the partial waves being searched actually varied somewhat over the energy band for each single-energy analysis and partial waves that were not searched sometimes had nonzero values. Contributions from unsearched waves were sometimes important at lower energies where the data were too few to support their direct determination.

These single-energy analyses are relatively form independent and are intended to compliment energy-dependent solution FP84; any systematic variations between the single-energy partial waves and those of solution FP84 would indicate structure not properly encoded by the energy-dependent fit. In fact, solution FP84 was developed, as described in Sec. VII, to include all such relevant structures.

We believe that the T-matrix errors given in Table IV are proper measures of the data-base uncertainties.

V. CHARGE CORRECTIONS FOR NUCLEAR PARTIAL-WAVE AMPLITUDES

Nuclear partial waves are modified by Coulomb-barrier factors for use in particular charge channels. We first extract a K matrix from the "nuclear" T matrix as

$$K_n=T_n/(1+iT_n) , \tag{7}$$

where T_n = nuclear T matrix. This K matrix is then multiplied by the appropriate barrier factor in order to calculate a "charge-corrected" T matrix:

$$\begin{aligned} T_c&=B_lK_n/(1-iB_lK_n) \\ &=B_lT_n/(1+iT_n-iB_lT_n) , \end{aligned} \tag{8}$$

where B_l is the usual Coulomb-barrier factor:

$$B_0=2\pi\eta/(e^{2\pi\eta}-1) ,$$

where $\eta=\pm\alpha/V_r$ for $\pi^{\pm}p$, α = fine-structure constant, V_r = (pion laboratory velocity)/c, and

$$B_l=B_0\prod_{j=1}^{l}[1+(\eta/j)^2] .$$

For charge-exchange reactions we use the square root of the π^-p barrier factor.

The dominant effect of these corrections is to suppress low-energy π^+p partial waves, while enhancing low-energy π^-p and charge-exchange partial waves. The effects, although nominal, are not small when measured against phase-shift errors obtained for the single-energy fits at low energies. This is illustrated in Table I, which is a tabulation of nuclear, π^+p, and π^-p phase shifts for the S_{31} and P_{33} states at the three lowest energies (30, 50, and 100 MeV). Differences between different charge channels are as large as seven standard deviations.

In order to measure the demand for charge splitting in the data, we compared single-energy analyses below 500 MeV which were done in the following ways:

(c) Combined (π^+p, π^-p, and CXS) data with both $I=\frac{1}{2}$ and $I=\frac{3}{2}$ waves searched (reported analyses).

(+) π^+p data only with $I=\frac{3}{2}$ wave searched.

(−) π^-p and CXS data with $I=\frac{1}{2}$ waves plus S_{31} and P_{33} waves searched.

TABLE I. Phase shifts at 30, 50, and 100 MeV for S_{31} and P_{33} as Coulomb corrected for various charge channels. (N) indicates uncorrected, (+) indicates corrected for π^+p scattering, and (−) indicates corrected for π^-p scattering. Phase shifts are in degrees. Analysis errors are indicated in parentheses beside the (N) values.

T_{lab}	30 MeV	50 MeV	100 MeV
S_{31} (N)	−3.39(0.07)	−5.25(0.09)	−8.86(0.11)
S_{31} (+)	−3.33	−5.07	−8.52
S_{31} (−)	−3.61	−5.43	−9.01
P_{33} (N)	2.50(0.03)	6.21(0.06)	22.37(0.05)
P_{33} (+)	2.46	6.00	21.80
P_{33} (−)	2.67	6.42	22.94

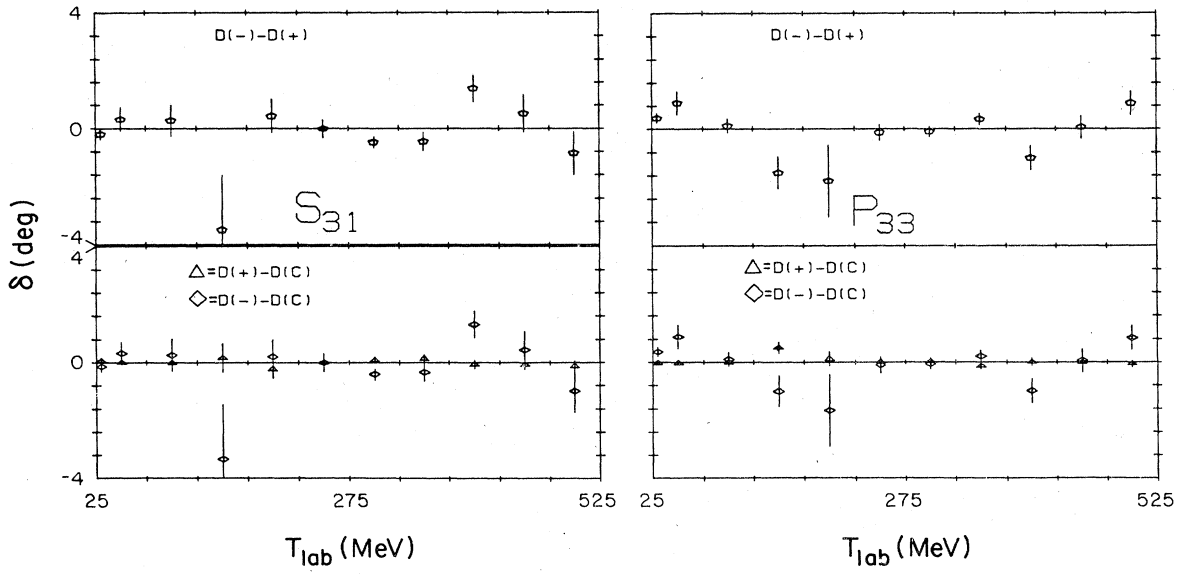

FIG. 4. Nuclear phase-shift differences for S_{31} and P_{33} at single energies below 500 MeV. δ_C indicates a phase shift obtained by fitting combined data by searching $I=\frac{1}{2}$ and $I=\frac{3}{2}$ waves; δ_+ indicates a phase shift obtained by fitting π^+p data only by searching $I=\frac{3}{2}$ waves; δ_- indicates a phase shift obtained by fitting π^-p and CXS data only by searching $I=\frac{1}{2}$ waves plus S_{31} and P_{33}. Plotted errors are from the $(-)$ analyses except for the difference, $\delta_+-\delta_C$, for which the $(+)$ errors were used.

For S_{31} and P_{33} we then compared the difference in nuclear phases, $\delta_+-\delta_c$, using errors from the $(+)$ analyses, with the difference in nuclear phases, $\delta_--\delta_c$, using errors from the $(-)$ analyses. These comparisons are plotted in Fig. 4, along with the difference in nuclear phases, $\delta_--\delta_+$, using errors from the $(-)$ analyses. If our Coulomb modifications are proper, all of these phase differences should be consistent with zero. We see nothing systematic in these results which would indicate that the data required further or different Coulomb modifications. Our conclusion from this comparison is that the modifications which we employ are necessary and sufficient to fit all charge channels with a single nuclear amplitude.

VI. LOW-ENERGY REPRESENTATION: SCATTERING LENGTHS

The low-energy behavior of our energy-dependent solution FP84 can be efficiently represented in terms of a "scattering-length" function defined by

$$[kA(k^2)]^{2l+1}=\tan\delta\,, \tag{9}$$

where k=center-of-mass momentum in inverse fm and δ=nuclear phase shift. At threshold $A(0)$ is just the conventional scattering length; its values for the S and P states are given in Table II. In Fig. 5 we plot the scattering-length functions $A(k^2)$ for S and P states below 100 MeV. It is apparent that the functions displayed can be well represented by linear functions of energy. The P_{33} state, of course, has a resonance at about 190 MeV, so its linearity would vanish quickly above 100 MeV.

Although it is customary to describe low-energy scattering in terms of scattering lengths, we feel that the full solution should be used for most calculations.

VII. PARTIAL-WAVE AMPLITUDES: CHARACTERIZING THE SOLUTIONS

Solution FP84 and the single-energy analyses reported in this paper were begun with an energy-dependent fit FA84 to the unpruned data base. A large number of iterations were performed between FA84 and the single-energy solutions to ensure that there were no structures suggested by the single-energy fits that were not encoded by the energy-dependent form. In the cycle, energy

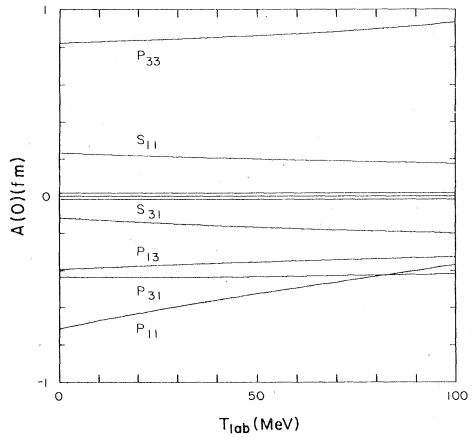

FIG. 5. Scattering-length function $A(k^2)$ for S and P waves from solution FP84 for 0—100-MeV laboratory kinetic energy.

TABLE II. Scattering lengths $A(k^2=0)$ from solution FP84.

State	S_{11}	S_{31}	P_{11}	P_{13}	P_{31}	P_{33}
A (fm)	0.23	−0.11	−0.71	−0.405	−0.459	0.815

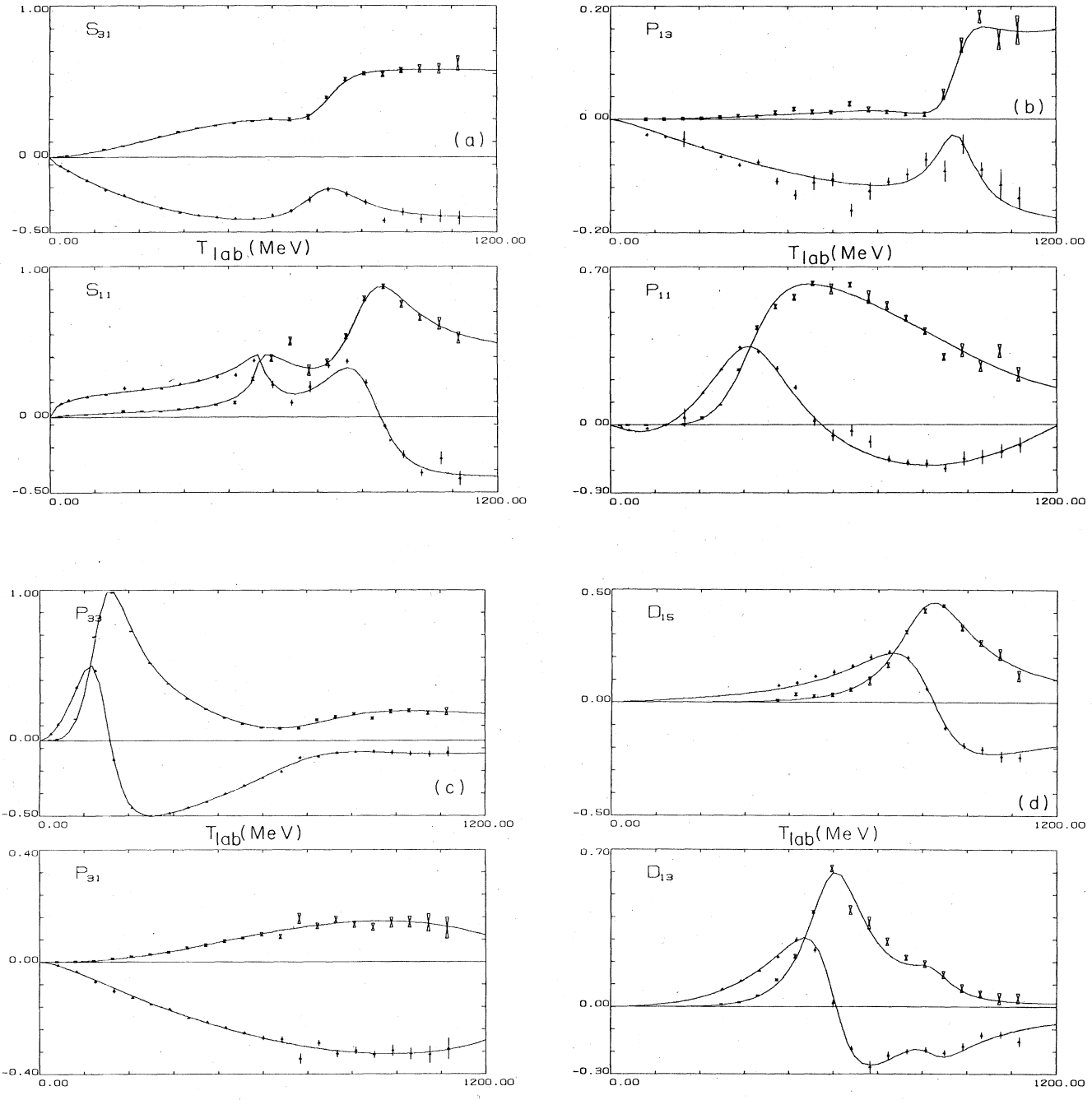

FIG. 6. Partial-wave amplitudes from solution FP84 and from the single-energy analyses. ReT is indicated by Δ while ImT is indicated by ×.

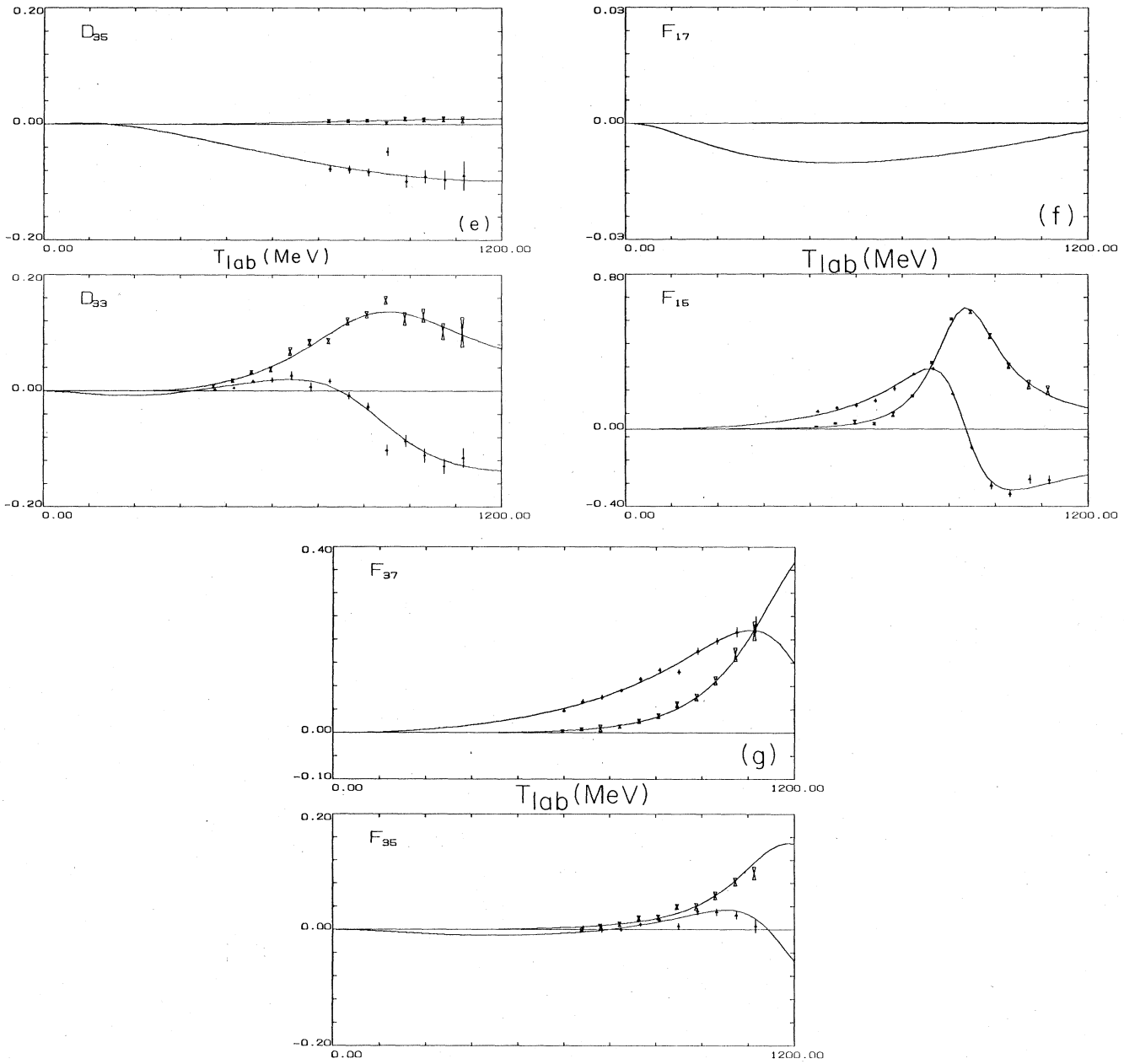

FIG. 6. (*Continued*).

derivatives and initial phase parameters were obtained from FA84 for generation of the single-energy fits. This procedure resulted in a solution FA84 containing 121 searched parameters: 64 for the 13 $I=\frac{1}{2}$ waves, and 57 for the 13 $I=\frac{3}{2}$ waves determined by these analyses.

After developing FA84, we examined the effects of pruning the data; a number of single data points contributed very large χ^2 contributions to FA84. We found that by pruning all data points with χ^2 contributions in excess of 16 (4 standard deviations), overall χ^2 could be reduced by about 20% (from 20 000 to 15 000), while less than 2% of the data were eliminated. The resultant solution, upon reanalysis, changed very slightly but exhibited superior numerical characteristics ("cleaner" searches).

Solution FP84 was developed by the pruning procedure described above: prune-search-prune-search, etc. The final result, reported in this paper, is a solution with 161 fewer data (9269 vs 9430) and a χ^2 of 15504 (vs 20136 for FA84). The two solutions are extremely close to each other, as one would expect from such a slight pruning of the data base. Although FA84 is not reported herein, it is encoded on the SAID facility (see below) and can be studied there.

We believe that the pruned data base provides a superior representation for πN scattering below 1100 MeV and, therefore, report solution FP84 as the best energy-

TABLE III. Nuclear partial-wave amplitudes from solution FP84. $T_r = \mathrm{Re}T_n$, $T_i = \mathrm{Im}T_n$.

(a) $I = \frac{1}{2}$

T_{lab} (MeV)	$W_{c.m.}$ (MeV)	$T_r(P_{11})T_i$	$T_r(D_{13})T_i$	$T_r(F_{15})T_i$	$T_r(G_{17})T_i$	$T_r(H_{19})T_i$	$T_r(I_{111})T_i$
30	1103	−0.015 0.000	0.001 0.000	−0.000 0.000	0.000 0.000	0.000 0.000	0.000 0.000
50	1120	−0.024 0.001	0.001 0.000	0.000 0.000	0.000 0.000	0.000 0.000	0.000 0.000
100	1161	−0.026 0.001	0.006 0.000	0.000 0.000	0.000 0.000	0.000 0.000	0.000 0.000
150	1201	0.001 0.000	0.014 0.000	0.002 0.000	0.001 0.000	0.000 0.000	0.000 0.000
200	1239	0.057 0.005	0.026 0.001	0.005 0.000	0.002 0.000	0.001 0.000	0.000 0.000
250	1277	0.143 0.030	0.045 0.003	0.010 0.000	0.004 0.000	0.002 0.000	0.000 0.000
300	1313	0.249 0.100	0.073 0.009	0.017 0.000	0.005 0.000	0.002 0.000	0.000 0.000
350	1348	0.337 0.242	0.112 0.021	0.026 0.001	0.006 0.000	0.003 0.000	0.000 0.000
400	1382	0.332 0.426	0.165 0.048	0.038 0.002	0.008 0.000	0.004 0.000	0.000 0.000
450	1416	0.239 0.560	0.231 0.105	0.053 0.005	0.010 0.001	0.004 0.000	0.000 0.000
500	1449	0.126 0.617	0.295 0.223	0.072 0.009	0.013 0.001	0.005 0.000	−0.000 0.000
550	1481	0.031 0.625	0.278 0.432	0.097 0.016	0.016 0.002	0.005 0.000	−0.000 0.000
600	1512	−0.041 0.608	0.048 0.597	0.128 0.028	0.019 0.003	0.006 0.000	−0.001 0.000
650	1543	−0.094 0.578	−0.199 0.501	0.169 0.051	0.023 0.003	0.006 0.000	−0.001 0.001
700	1573	−0.132 0.542	−0.262 0.334	0.222 0.094	0.028 0.005	0.007 0.000	−0.001 0.001
750	1602	−0.157 0.502	−0.236 0.230	0.281 0.179	0.033 0.006	0.007 0.000	−0.002 0.001
800	1631	−0.173 0.458	−0.198 0.189	0.310 0.342	0.039 0.007	0.007 0.000	−0.002 0.002
850	1660	−0.178 0.414	−0.198 0.183	0.192 0.559	0.045 0.009	0.008 0.000	−0.002 0.003
900	1688	−0.174 0.370	−0.223 0.128	−0.090 0.613	0.051 0.011	0.008 0.000	−0.003 0.003
950	1715	−0.163 0.326	−0.194 0.067	−0.272 0.470	0.059 0.013	0.008 0.000	−0.003 0.004
1000	1743	−0.143 0.285	−0.156 0.039	−0.314 0.326	0.066 0.015	0.008 0.000	−0.004 0.005
1050	1769	−0.116 0.248	−0.126 0.026	−0.303 0.232	0.074 0.018	0.008 0.000	−0.004 0.007
1100	1796	−0.084 0.215	−0.104 0.020	−0.280 0.173	0.083 0.021	0.009 0.000	−0.005 0.008
	No. of searched parameters	6	9	6	4	2	3

T_{lab} (MeV)	$W_{c.m.}$ (MeV)	$T_r(S_{11})T_i$	$T_r(P_{13})T_i$	$T_r(D_{15})T_i$	$T_r(F_{17})T_i$	$T_r(G_{19})T_i$	$T_r(H_{111})T_i$	$T_r(I_{113})T_i$
30	1103	0.088 0.008	−0.004 0.000	0.001 0.000	−0.000 0.000	−0.000 0.000	−0.000 0.000	−0.000 0.000
50	1120	0.108 0.012	−0.007 0.000	0.002 0.000	−0.000 0.000	−0.000 0.000	−0.000 0.000	−0.000 0.000
100	1161	0.138 0.019	−0.018 0.000	0.006 0.000	−0.002 0.000	−0.001 0.000	−0.000 0.000	−0.000 0.000
150	1201	0.156 0.025	−0.029 0.001	0.011 0.000	−0.003 0.000	−0.002 0.000	−0.001 0.000	−0.000 0.000
200	1239	0.169 0.029	−0.040 0.002	0.016 0.000	−0.005 0.000	−0.003 0.000	−0.002 0.000	−0.000 0.000
250	1277	0.181 0.034	−0.050 0.003	0.022 0.001	−0.007 0.000	−0.004 0.000	−0.002 0.000	−0.001 0.000
300	1313	0.196 0.041	−0.061 0.004	0.028 0.001	−0.008 0.000	−0.005 0.000	−0.003 0.000	−0.001 0.000
350	1348	0.215 0.050	−0.070 0.005	0.036 0.002	−0.009 0.000	−0.005 0.000	−0.003 0.000	−0.001 0.000
400	1382	0.241 0.064	−0.080 0.006	0.046 0.004	−0.010 0.000	−0.005 0.000	−0.003 0.000	−0.000 0.000
450	1416	0.277 0.088	−0.088 0.008	0.059 0.007	−0.010 0.000	−0.004 0.000	−0.003 0.000	0.000 0.000
500	1449	0.330 0.134	−0.096 0.010	0.074 0.012	−0.010 0.000	−0.002 0.001	−0.002 0.000	0.001 0.000
550	1481	0.417 0.268	−0.102 0.012	0.095 0.021	−0.010 0.000	−0.000 0.001	−0.000 0.000	0.001 0.000
600	1512	0.221 0.407	−0.108 0.013	0.121 0.036	−0.010 0.000	0.002 0.002	0.001 0.001	0.002 0.000
650	1543	0.153 0.354	−0.113 0.015	0.153 0.063	−0.010 0.000	0.005 0.003	0.003 0.001	0.003 0.000
700	1573	0.178 0.325	−0.116 0.015	0.190 0.111	−0.009 0.000	0.008 0.004	0.006 0.002	0.005 0.000
750	1602	0.258 0.364	−0.115 0.014	0.217 0.196	−0.009 0.000	0.012 0.006	0.008 0.002	0.006 0.000
800	1631	0.327 0.532	−0.109 0.012	0.192 0.324	−0.008 0.000	0.016 0.008	0.011 0.003	0.007 0.000
850	1660	0.213 0.786	−0.087 0.011	0.066 0.431	−0.008 0.000	0.020 0.011	0.014 0.005	0.009 0.000
900	1688	−0.063 0.864	−0.041 0.039	−0.098 0.422	−0.007 0.000	0.024 0.014	0.018 0.006	0.010 0.000
950	1715	−0.252 0.776	−0.041 0.130	−0.194 0.337	−0.006 0.000	0.028 0.017	0.021 0.008	0.012 0.000
1000	1743	−0.335 0.674	−0.105 0.164	−0.224 0.253	−0.005 0.000	0.033 0.021	0.025 0.010	0.014 0.000
1050	1769	−0.369 0.600	−0.140 0.160	−0.225 0.192	−0.004 0.000	0.037 0.026	0.029 0.012	0.016 0.000
1100	1796	−0.383 0.550	−0.157 0.156	−0.215 0.151	−0.003 0.000	0.042 0.031	0.033 0.014	0.018 0.000
No. of searched parameters		9	7	7	3	3	3	2

TABLE III. (*Continued*).

(b) $I=\frac{3}{2}$

T_{lab} (MeV)	$W_{c.m.}$ (MeV)	$T_r(P_{31})T_i$	$T_r(D_{33})T_i$	$T_r(F_{35})T_i$	$T_r(G_{37})T_i$	$T_{r(H_{39})}T_i$	$T_r(I_{311})T_i$
30	1103	−0.006 0.000	−0.000 0.000	−0.000 0.000	−0.000 0.000	−0.000 0.000	0.000 0.000
50	1120	−0.013 0.000	−0.001 0.000	−0.000 0.000	−0.000 0.000	−0.000 0.000	0.000 0.000
100	1161	−0.037 0.001	−0.004 0.000	−0.002 0.000	−0.000 0.000	−0.000 0.000	0.000 0.000
150	1201	−0.065 0.004	−0.006 0.000	−0.004 0.000	−0.001 0.000	−0.000 0.000	0.000 0.000
200	1239	−0.093 0.009	−0.008 0.000	−0.005 0.000	−0.001 0.000	−0.001 0.000	0.000 0.000
250	1277	−0.122 0.016	−0.008 0.000	−0.007 0.000	−0.002 0.000	−0.001 0.000	0.000 0.000
300	1313	−0.148 0.025	−0.006 0.001	−0.008 0.000	−0.002 0.000	−0.001 0.000	0.000 0.000
350	1348	−0.173 0.036	−0.003 0.002	−0.009 0.000	−0.002 0.000	−0.001 0.000	0.001 0.000
400	1382	−0.196 0.048	0.001 0.006	−0.010 0.001	−0.002 0.000	−0.001 0.000	0.001 0.000
450	1416	−0.217 0.062	0.006 0.012	−0.010 0.001	−0.002 0.000	−0.001 0.000	0.001 0.000
500	1449	−0.237 0.075	0.011 0.020	−0.009 0.002	−0.002 0.000	−0.001 0.000	0.001 0.000
550	1481	−0.255 0.089	0.015 0.030	−0.008 0.003	−0.002 0.000	−0.000 0.000	0.002 0.000
600	1512	−0.271 0.101	0.019 0.043	−0.006 0.004	−0.001 0.000	0.001 0.000	0.002 0.000
650	1543	−0.286 0.113	0.020 0.059	−0.004 0.005	−0.001 0.000	0.001 0.000	0.002 0.000
700	1573	−0.298 0.123	0.017 0.078	−0.001 0.007	0.000 0.000	0.002 0.000	0.003 0.001
750	1602	−0.308 0.131	0.008 0.099	0.003 0.010	0.001 0.000	0.003 0.000	0.003 0.001
800	1631	−0.317 0.138	−0.009 0.119	0.008 0.014	0.001 0.000	0.004 0.000	0.004 0.001
850	1660	−0.323 0.143	−0.032 0.132	0.014 0.020	0.002 0.000	0.005 0.000	0.004 0.001
900	1688	−0.326 0.145	−0.059 0.137	0.021 0.029	0.003 0.000	0.006 0.000	0.005 0.002
950	1715	−0.328 0.145	−0.084 0.133	0.028 0.042	0.004 0.000	0.007 0.000	0.005 0.002
1000	1743	−0.326 0.142	−0.104 0.123	0.033 0.061	0.005 0.000	0.009 0.000	0.006 0.003
1050	1769	−0.321 0.135	−0.119 0.110	0.033 0.087	0.006 0.000	0.010 0.000	0.006 0.004
1100	1796	−0.312 0.125	−0.128 0.096	0.019 0.119	0.007 0.000	0.011 0.000	0.007 0.004
	No. of searched parameters	6	6	4	2	2	3

T_{lab} (MeV)	$W_{c.m.}$ (MeV)	$T_r(S_{31})T_i$	$T_r(P_{33})T_i$	$T_r(D_{35})T_i$	$T_r(F_{37})T_i$	$T_r(G_{39})T_i$	$T_r(H_{311})T_i$	$T_r(I_{313})T_i$
30	1103	−0.062 0.004	0.043 0.002	0.000 0.000	0.000 0.000	0.000 0.000	−0.000 0.000	0.000 0.000
50	1120	−0.090 0.008	0.102 0.010	0.001 0.000	0.000 0.000	0.000 0.000	−0.000 0.000	0.000 0.000
100	1161	−0.154 0.024	0.350 0.143	0.002 0.000	0.001 0.000	0.001 0.000	−0.000 0.000	0.000 0.000
150	1201	−0.211 0.047	0.462 0.691	0.001 0.000	0.002 0.000	0.001 0.000	−0.000 0.000	0.000 0.000
200	1239	−0.261 0.073	−0.125 0.984	−0.002 0.000	0.005 0.000	0.002 0.000	0.000 0.000	0.000 0.000
250	1277	−0.303 0.102	−0.446 0.726	−0.006 0.000	0.008 0.000	0.003 0.000	0.000 0.000	0.001 0.000
300	1313	−0.338 0.132	−0.500 0.509	−0.011 0.000	0.012 0.000	0.003 0.000	0.000 0.000	0.001 0.000
350	1348	−0.366 0.161	−0.483 0.370	−0.017 0.000	0.016 0.000	0.004 0.000	0.001 0.000	0.001 0.000
400	1382	−0.388 0.187	−0.447 0.276	−0.024 0.001	0.021 0.001	0.004 0.000	0.001 0.000	0.001 0.000
450	1416	−0.404 0.210	−0.404 0.206	−0.031 0.001	0.027 0.001	0.003 0.000	0.001 0.000	0.001 0.000
500	1449	−0.413 0.228	−0.356 0.153	−0.038 0.001	0.035 0.002	0.003 0.000	0.002 0.000	0.001 0.000
550	1481	−0.414 0.239	−0.302 0.114	−0.045 0.002	0.043 0.003	0.002 0.000	0.003 0.000	0.001 0.000
600	1512	−0.400 0.242	−0.244 0.090	−0.051 0.003	0.053 0.005	0.001 0.000	0.004 0.001	0.001 0.000
650	1543	−0.358 0.242	−0.186 0.084	−0.058 0.003	0.064 0.007	−0.000 0.000	0.005 0.001	0.000 0.000
700	1573	−0.276 0.273	−0.135 0.096	−0.064 0.004	0.077 0.011	−0.001 0.001	0.006 0.002	−0.000 0.000
750	1602	−0.210 0.386	−0.099 0.121	−0.070 0.005	0.092 0.016	−0.003 0.001	0.007 0.002	−0.000 0.000
800	1631	−0.242 0.504	−0.080 0.149	−0.076 0.006	0.109 0.025	−0.004 0.001	0.008 0.003	−0.001 0.000
850	1660	−0.302 0.555	−0.075 0.171	−0.081 0.007	0.129 0.036	−0.006 0.002	0.010 0.004	−0.002 0.000
900	1688	−0.343 0.571	−0.077 0.186	−0.085 0.007	0.151 0.053	−0.007 0.002	0.011 0.006	−0.002 0.001
950	1715	−0.367 0.576	−0.081 0.193	−0.089 0.008	0.174 0.078	−0.009 0.003	0.013 0.007	−0.003 0.001
1000	1743	−0.382 0.578	−0.085 0.195	−0.092 0.009	0.198 0.114	−0.011 0.004	0.015 0.009	−0.004 0.001
1050	1769	−0.390 0.578	−0.088 0.193	−0.094 0.009	0.215 0.163	−0.012 0.004	0.016 0.011	−0.004 0.001
1100	1796	−0.396 0.577	−0.088 0.189	−0.096 0.010	0.220 0.227	−0.014 0.005	0.018 0.013	−0.005 0.001
No. of searched parameters		8	8	4	5	3	3	3

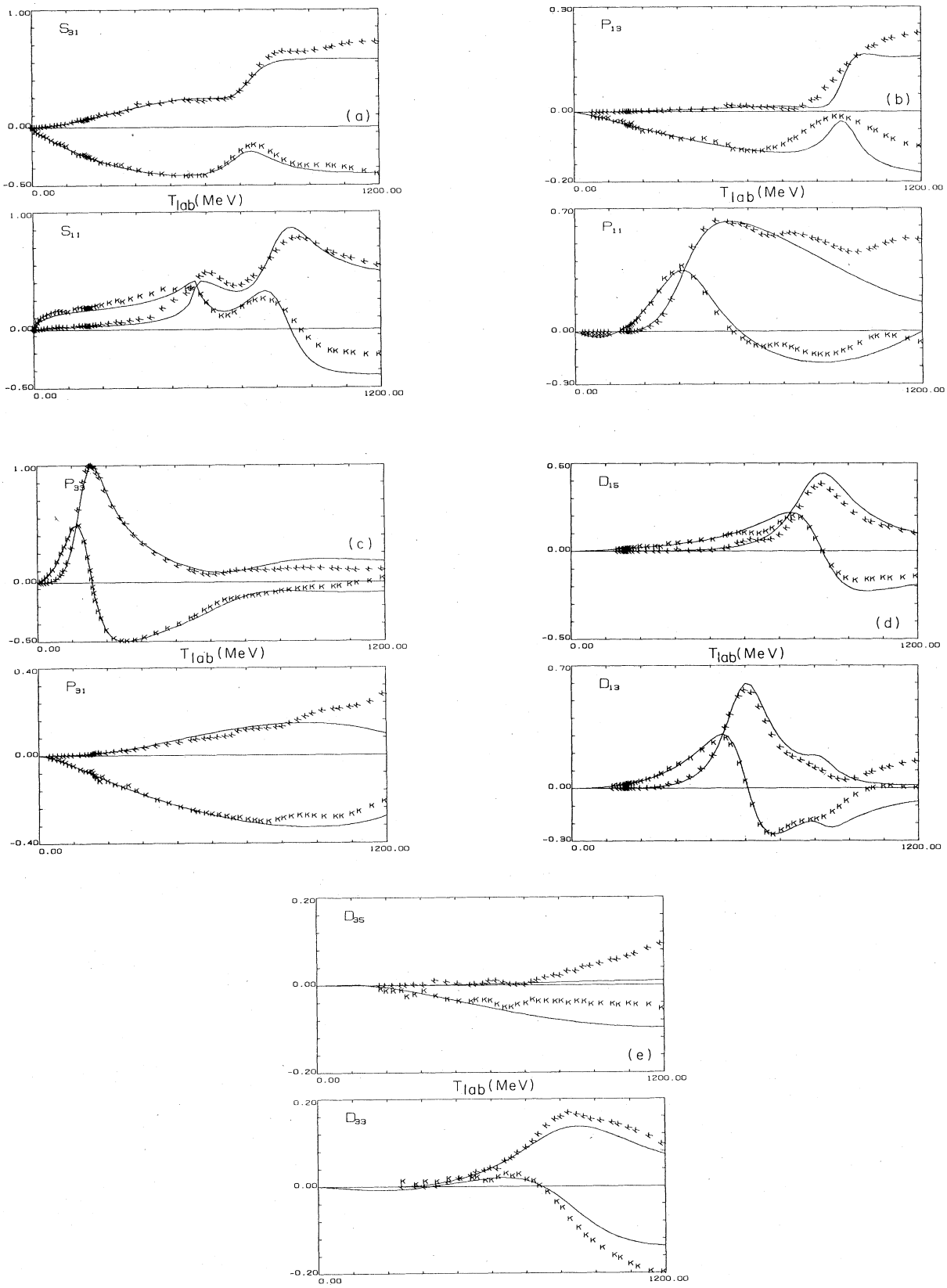

FIG. 7. Partial-wave amplitudes from solution FP84 plotted against the Karlsruhe-Helsinki solution. A vertical K is used to denote Re T while a slanted K denotes Im T.

TABLE IV. Searched partial waves from single-energy analyses. Each solution is characterized by a binning range (in parentheses), by the number of searched parameters (N_{par}), χ^2, and the number of data (N_{data}) used for analysis. The two numbers listed for χ^2(ED) are the χ^2 for FP84 for the selected data set and the χ^2 after linearizing and before searching FP84.

C3, $T_{lab}=30$ MeV (20–40), $N_{data}=125$, $N_{par}=4$, $\chi^2=168$, χ^2(ED)=(179,194)

Wave	ReT	ImT
S_{11}	0.090±0.001	0.008±0.002
S_{31}	−0.060±0.001	0.004±0.002
P_{11}	−0.011±0.001	0.000±0.002
P_{33}	0.043±0.001	0.002±0.002

C5, $T_{lab}=50$ MeV (35–65), $N_{data}=168$, $N_{par}=5$, $\chi^2=294$, χ^2(ED)=(293,321)

Wave	ReT	ImT
S_{11}	0.113±0.002	0.013±0.002
S_{31}	−0.092±0.002	0.009±0.002
P_{11}	−0.024±0.001	0.001±0.002
P_{31}	−0.013±0.001	0.000±0.002
P_{33}	0.107±0.001	0.012±0.002

C10, $T_{lab}=100$ MeV (88–110), $N_{data}=128$, $N_{par}=6$, $\chi^2=182$, χ^2(ED)=(205,271)

Wave	ReT	ImT
S_{11}	0.136±0.003	0.019±0.003
S_{31}	−0.154±0.002	0.024±0.002
P_{11}	−0.015±0.003	0.000±0.003
P_{13}	−0.027±0.002	0.001±0.002
P_{31}	−0.034±0.001	0.001±0.002
P_{33}	0.351±0.002	0.144±0.002

C15, $T_{lab}=150$ MeV (140–160), $N_{data}=67$, $N_{par}=6$, $\chi^2=126$, χ^2(ED)=(140,144)

Wave	ReT	ImT
S_{11}	0.150±0.003	0.023±0.003
S_{31}	−0.218±0.008	0.050±0.004
P_{11}	0.001±0.005	0.000±0.003
P_{13}	−0.030±0.003	0.001±0.003
P_{31}	−0.069±0.006	0.005±0.003
P_{33}	0.463±0.002	0.689±0.002

C20, $T_{lab}=200$ MeV (190–210), $N_{data}=71$, $N_{par}=6$, $\chi^2=103$, χ^2(ED)=(110,111)

Wave	ReT	ImT
S_{11}	0.193±0.013	0.039±0.006
S_{31}	−0.256±0.004	0.071±0.003
P_{11}	0.033±0.038	0.003±0.004
P_{13}	−0.035±0.014	0.001±0.003
P_{31}	−0.103±0.007	0.011±0.003
P_{33}	−0.126±0.006	0.984±0.003

C25, $T_{lab}=250$ MeV (240–265), $N_{data}=168$, $N_{par}=6$, $\chi^2=276$, χ^2(ED)=(298,315)

Wave	ReT	ImT
S_{11}	0.191±0.004	0.038±0.003
S_{31}	−0.300±0.002	0.101±0.002
P_{11}	0.143±0.004	0.031±0.005
P_{13}	−0.048±0.002	0.002±0.002
P_{31}	−0.128±0.003	0.018±0.003
P_{33}	−0.447±0.002	0.725±0.002

C30, $T_{lab}=300$ MeV (285–315), $N_{data}=333$, $N_{par}=8$, $\chi^2=445$, χ^2(ED)=(488,492)

Wave	ReT	ImT
S_{11}	0.190±0.002	0.038±0.002
S_{31}	−0.339±0.002	0.134±0.002
P_{11}	0.247±0.002	0.088±0.003
P_{13}	−0.065±0.002	0.004±0.002
P_{31}	−0.151±0.002	0.026±0.003
P_{33}	−0.500±0.002	0.515±0.002
D_{13}	0.077±0.002	0.009±0.003

C35, $T_{lab}=350$ MeV (330–370), $N_{data}=248$, $N_{par}=9$, $\chi^2=410$, χ^2(ED)=(442,447)

Wave	ReT	ImT
S_{11}	0.220±0.004	0.052±0.003
S_{31}	−0.370±0.002	0.164±0.002
P_{11}	0.344±0.004	0.245±0.004
P_{13}	−0.080±0.003	0.006±0.003
P_{31}	−0.169±0.003	0.035±0.004
P_{33}	−0.484±0.002	0.376±0.002
D_{13}	0.116±0.002	0.019±0.003

C40, $T_{lab}=400$ MeV (375–425) $N_{data}=348$, $N_{par}=9$, $\chi^2=648$, χ^2(ED)=(673,671)

Wave	ReT	ImT
S_{11}	0.243±0.007	0.066±0.004
S_{31}	−0.390±0.003	0.189±0.002
P_{11}	0.326±0.006	0.432±0.008
P_{13}	−0.075±0.005	0.006±0.003
P_{31}	−0.200±0.003	0.050±0.004
P_{33}	−0.447±0.002	0.276±0.002
D_{13}	0.160±0.002	0.049±0.003

TABLE IV. (*Continued*).

C45, $T_{lab}=450$ MeV (425–475), $N_{data}=245$, $N_{par}=12$, $\chi^2=385$, χ^2(ED)=(460,472)		
Wave	ReT	ImT
S_{11}	0.267±0.008	0.082±0.006
S_{31}	−0.401±0.003	0.206±0.003
P_{11}	0.252±0.008	0.525±0.009
P_{13}	−0.109±0.006	0.012±0.003
P_{31}	−0.214±0.003	0.061±0.005
P_{33}	−0.406±0.002	0.209±0.002
D_{13}	0.221±0.004	0.119±0.005
D_{15}	0.073±0.003	0.009±0.003
D_{33}	0.003±0.002	0.008±0.003

C50, $T_{lab}=500$ MeV (475–525), $N_{data}=441$, $N_{par}=14$, $\chi^2=773$, χ^2(ED)=(837,882)		
Wave	ReT	ImT
S_{11}	0.282±0.011	0.096±0.009
S_{31}	−0.409±0.004	0.221±0.003
P_{11}	0.168±0.009	0.568±0.013
P_{13}	−0.133±0.008	0.019±0.003
P_{31}	−0.234±0.004	0.074±0.006
P_{33}	−0.353±0.003	0.150±0.003
D_{13}	0.299±0.009	0.225±0.008
D_{15}	0.087±0.006	0.036±0.007
D_{33}	0.006±0.002	0.018±0.003
F_{15}	0.089±0.004	0.012±0.003

C55, $T_{lab}=550$ MeV (535–565), $N_{data}=395$, $N_{par}=18$, $\chi^2=568$, χ^2(ED)=(631,715)		
Wave	ReT	ImT
S_{11}	0.376±0.010	0.255±0.013
S_{31}	−0.411±0.005	0.236±0.004
P_{11}	0.018±0.020	0.629±0.010
P_{13}	−0.111±0.013	0.014±0.004
P_{31}	−0.252±0.004	0.086±0.003
P_{33}	−0.301±0.003	0.110±0.003
D_{13}	0.253±0.010	0.422±0.006
D_{15}	0.115±0.005	0.028±0.006
D_{33}	0.017±0.002	0.033±0.003
F_{15}	0.109±0.004	0.029±0.005

C60, $T_{lab}=600$ MeV (585–615), $N_{data}=322$, $N_{par}=20$, $\chi^2=458$, χ^2(ED)=(517,521)		
Wave	ReT	ImT
S_{11}	0.214±0.022	0.392±0.023
S_{31}	−0.387±0.006	0.250±0.006
P_{11}	−0.046±0.024	0.604±0.022
P_{13}	−0.105±0.011	0.013±0.003
P_{31}	−0.269±0.008	0.099±0.006
P_{33}	−0.248±0.004	0.087±0.004
D_{13}	0.017±0.011	0.616±0.015
D_{15}	0.134±0.009	0.032±0.008
D_{33}	0.019±0.004	0.037±0.004
F_{15}	0.123±0.010	0.036±0.011
F_{37}	0.047±0.002	0.004±0.003

C65, $T_{lab}=650$ MeV (635–665), $N_{data}=285$, $N_{par}=23$, $\chi^2=478$, χ^2(ED)=(579,566)		
Wave	ReT	ImT
S_{11}	0.096±0.018	0.506±0.026
S_{31}	−0.357±0.011	0.248±0.010
P_{11}	−0.026±0.024	0.623±0.011
P_{13}	−0.160±0.011	0.028±0.004
P_{31}	−0.274±0.010	0.090±0.008
P_{33}	−0.206±0.007	0.082±0.006
D_{13}	−0.186±0.012	0.431±0.019
D_{15}	0.163±0.007	0.056±0.008
D_{33}	0.027±0.008	0.068±0.007
F_{15}	0.147±0.008	0.028±0.006
F_{35}	0.003±0.004	0.000±0.003
F_{37}	0.068±0.004	0.008±0.003
G_{19}	0.015±0.004	0.003±0.003

C70, $T_{lab}=700$ MeV (685–715), $N_{data}=246$, $N_{par}=27$, $\chi^2=342$, χ^2(ED)=(434,441)		
Wave	ReT	ImT
S_{11}	0.202±0.037	0.311±0.036
S_{31}	−0.284±0.020	0.262±0.017
P_{11}	−0.073±0.027	0.568±0.027
P_{13}	−0.126±0.015	0.018±0.005
P_{31}	−0.344±0.018	0.156±0.018
P_{33}	−0.112±0.009	0.083±0.005
D_{13}	−0.269±0.026	0.374±0.027
D_{15}	0.201±0.012	0.093±0.019
D_{33}	0.008±0.007	0.084±0.006
F_{15}	0.207±0.011	0.076±0.011
F_{35}	0.001±0.006	0.005±0.005
F_{37}	0.077±0.004	0.010±0.007
G_{17}	0.028±0.008	0.005±0.018
G_{19}	0.006±0.005	0.000±0.003

TABLE IV. (*Continued*).

C75, $T_{lab}=750$ MeV (730–770), $N_{data}=448$, $N_{par}=28$, $\chi^2=584$, $\chi^2(ED)=(670,664)$

Wave	ReT	ImT
S_{11}	0.343±0.018	0.365±0.022
S_{31}	−0.214±0.014	0.393±0.008
P_{11}	−0.150±0.013	0.530±0.018
P_{13}	−0.110±0.007	0.013±0.003
P_{31}	−0.289±0.010	0.129±0.010
P_{33}	−0.105±0.005	0.138±0.006
D_{13}	−0.216±0.016	0.290±0.016
D_{15}	0.224±0.009	0.165±0.012
D_{33}	0.018±0.004	0.086±0.005
D_{35}	−0.076±0.005	0.006±0.003
F_{15}	0.283±0.006	0.170±0.006
F_{35}	0.001±0.003	0.010±0.004
F_{37}	0.091±0.003	0.014±0.004
G_{17}	0.015±0.008	0.006±0.010
G_{19}	0.005±0.003	0.002±0.004

C80, $T_{lab}=800$ MeV (785–815), $N_{data}=415$, $N_{par}=28$, $\chi^2=607$, $\chi^2(ED)=(712,704)$

Wave	ReT	ImT
S_{11}	0.372±0.015	0.536±0.017
S_{31}	−0.247±0.017	0.517±0.011
P_{11}	−0.165±0.013	0.475±0.012
P_{13}	−0.096±0.010	0.010±0.003
P_{31}	−0.327±0.012	0.150±0.012
P_{33}	−0.081±0.007	0.159±0.008
D_{13}	−0.200±0.011	0.219±0.012
D_{15}	0.198±0.008	0.312±0.008
D_{33}	−0.008±0.006	0.120±0.007
D_{35}	−0.077±0.007	0.006±0.003
F_{15}	0.311±0.007	0.344±0.006
F_{35}	0.009±0.003	0.019±0.004
F_{37}	0.116±0.003	0.026±0.004
G_{17}	0.024±0.007	0.006±0.007
G_{19}	0.015±0.003	0.001±0.004

C85, $T_{lab}=850$ MeV (830–870), $N_{data}=439$, $N_{par}=28$, $\chi^2=664$, $\chi^2(ED)=(716,795)$

Wave	ReT	ImT
S_{11}	0.231±0.017	0.786±0.017
S_{31}	−0.299±0.017	0.552±0.013
P_{11}	−0.170±0.016	0.417±0.015
P_{13}	−0.070±0.012	0.009±0.004
P_{31}	−0.316±0.012	0.134±0.012
P_{33}	−0.073±0.007	0.177±0.009
D_{13}	−0.192±0.012	0.190±0.015
D_{15}	0.061±0.007	0.407±0.010
D_{33}	−0.026±0.006	0.131±0.006
D_{35}	−0.082±0.006	0.007±0.003
F_{15}	0.181±0.006	0.568±0.006
F_{35}	0.017±0.003	0.022±0.004
F_{37}	0.136±0.003	0.036±0.005
G_{17}	0.040±0.007	0.003±0.003
G_{19}	0.024±0.005	0.016±0.004

C90, $T_{lab}=900$ MeV (880–920), $N_{data}=484$, $N_{par}=29$, $\chi^2=612$, $\chi^2(ED)=(755,849)$

Wave	ReT	ImT
S_{11}	−0.059±0.014	0.867±0.016
S_{31}	−0.421±0.017	0.547±0.017
P_{11}	−0.191±0.015	0.302±0.015
P_{13}	−0.091±0.018	0.045±0.009
P_{31}	−0.330±0.013	0.125±0.013
P_{33}	−0.073±0.010	0.147±0.009
D_{13}	−0.204±0.012	0.143±0.016
D_{15}	−0.112±0.008	0.429±0.006
D_{33}	−0.101±0.009	0.157±0.007
D_{35}	−0.046±0.007	0.002±0.003
F_{15}	−0.095±0.008	0.604±0.008
F_{35}	0.006±0.005	0.040±0.004
F_{37}	0.131±0.005	0.061±0.006
G_{17}	0.031±0.008	0.011±0.007
G_{19}	0.018±0.007	0.023±0.003

C95, $T_{lab}=950$ MeV (925–975), $N_{data}=604$, $N_{par}=34$, $\chi^2=722$, $\chi^2(ED)=(834,911)$

Wave	ReT	ImT
S_{11}	−0.249±0.023	0.751±0.023
S_{31}	−0.364±0.024	0.573±0.018
P_{11}	−0.148±0.030	0.331±0.028
P_{13}	−0.043±0.017	0.131±0.013
P_{31}	−0.316±0.018	0.140±0.018
P_{33}	−0.079±0.013	0.193±0.012
D_{13}	−0.176±0.015	0.082±0.018
D_{15}	−0.188±0.013	0.330±0.013
D_{33}	−0.085±0.010	0.125±0.011
D_{35}	−0.097±0.011	0.010±0.003
F_{15}	−0.292±0.016	0.479±0.013
F_{35}	0.032±0.006	0.040±0.005
F_{37}	0.176±0.007	0.076±0.007
G_{17}	0.058±0.007	0.009±0.007
G_{19}	0.014±0.006	0.018±0.005
G_{39}	−0.008±0.006	0.003±0.003
H_{111}	0.023±0.006	0.011±0.005
H_{311}	0.017±0.004	0.007±0.004

C99, $T_{lab}=999$ MeV (970–1030), $N_{data}=572$, $N_{par}=35$, $\chi^2=785$, $\chi^2(ED)=(942,992)$

Wave	ReT	ImT
S_{11}	−0.370±0.022	0.659±0.021
S_{31}	−0.409±0.025	0.584±0.026
P_{11}	−0.141±0.030	0.261±0.024
P_{13}	−0.088±0.012	0.182±0.011
P_{31}	−0.327±0.020	0.143±0.020
P_{33}	−0.085±0.014	0.198±0.011
D_{13}	−0.127±0.012	0.057±0.014
D_{15}	−0.207±0.014	0.263±0.014
D_{33}	−0.110±0.012	0.130±0.012
D_{35}	−0.090±0.011	0.008±0.003
F_{15}	−0.335±0.014	0.326±0.013
F_{35}	0.030±0.006	0.058±0.007
F_{37}	0.197±0.006	0.112±0.009
G_{17}	0.060±0.006	0.022±0.009
G_{19}	0.018±0.006	0.018±0.005
G_{39}	−0.010±0.006	0.001±0.006
H_{111}	0.012±0.006	0.007±0.007
H_{311}	0.017±0.005	0.006±0.004

TABLE IV. (*Continued*).

C105, $T_{lab}=1050$ MeV (1020–1080) $N_{data}=680$, $N_{par}=35$, $\chi^2=943$, χ^2(ED)=(1072,1068)			C110, $T_{lab}=1100$ MeV (1080–1120), $N_{data}=420$, $N_{par}=35$, $\chi^2=730$, χ^2(ED)=(945,945)		
Wave	ReT	ImT	Wave	ReT	ImT
S_{11}	−0.272±0.041	0.622±0.040	S_{11}	−0.406±0.044	0.526±0.037
S_{31}	−0.391±0.042	0.585±0.032	S_{31}	−0.403±0.045	0.619±0.048
P_{11}	−0.116±0.029	0.329±0.029	P_{11}	−0.089±0.033	0.224±0.030
P_{13}	−0.115±0.026	0.142±0.018	P_{13}	−0.138±0.019	0.159±0.025
P_{31}	−0.330±0.030	0.140±0.031	P_{31}	−0.309±0.037	0.122±0.038
P_{33}	−0.090±0.020	0.184±0.012	P_{33}	−0.075±0.032	0.193±0.023
D_{13}	−0.124±0.014	0.035±0.025	D_{13}	−0.155±0.019	0.038±0.022
D_{15}	−0.237±0.023	0.214±0.024	D_{15}	−0.240±0.019	0.118±0.024
D_{33}	−0.129±0.013	0.103±0.014	D_{33}	−0.114±0.017	0.102±0.026
D_{35}	−0.095±0.016	0.009±0.004	D_{35}	−0.088±0.025	0.008±0.005
F_{15}	−0.257±0.022	0.230±0.022	F_{15}	−0.261±0.020	0.199±0.022
F_{35}	0.025±0.006	0.083±0.007	F_{35}	0.006±0.011	0.098±0.011
F_{37}	0.216±0.010	0.168±0.014	F_{37}	0.233±0.017	0.219±0.020
G_{17}	0.074±0.006	0.055±0.013	G_{17}	0.078±0.007	0.042±0.010
G_{19}	0.041±0.007	0.018±0.009	G_{19}	0.063±0.007	0.020±0.009
G_{39}	−0.012±0.006	0.004±0.006	G_{39}	−0.013±0.011	0.017±0.012
H_{111}	0.019±0.006	0.002±0.006	H_{111}	0.020±0.006	0.002±0.007
H_{311}	0.019±0.003	0.015±0.005	H_{311}	0.023±0.007	0.013±0.008

dependent fit. Characterized by charge channel, FP84 resulted in the following χ^2/data: $\pi^+p=5708/3709$, $\pi^-p=8267/4860$, and CXS$=1528/700$.

In Fig. 6 we plot the partial waves of solution FP84 for 0—1200 MeV (our FP84 analysis end point is 1100 MeV), along with the results of our single-energy analyses. In Table III the partial-wave amplitudes of solution FP84 are tabulated at those energies where single-energy fits were obtained. As we have indicated throughout this report, agreement between FP84 and the single-energy fits is convincing of a consistent picture (Figs. 6 and 7).

In Table IV we present partial waves, with errors, for the single-energy analyses. Only those partial waves with searched parameters are given; other waves taken from FP84 are given in Table III.

Figure 8 is a brief summary of how well the FP84 solution fits the angular data. Figures 2 and 3 show the fits for energy data.

Our method of parametrizing FP84 allows us to analytically continue the partial-wave amplitudes into the complex total-energy (W) plane and to locate the structures, poles and zeros, which give the on-shell features shown in Fig. 6. In Table V we enumerate the complex-plane positions (Re W, Im W) for poles and zeros of all partial waves through $l=3$ and for $1300\leq \mathrm{Re}\,W\leq 1900$ MeV and $-200\leq \mathrm{Im}\,W\leq 0$ MeV. In addition to the poles and zeros of Table V, on-shell structure is strongly influenced by the $\pi\Delta$ branch cut which starts at $W=(1360,-51)$ MeV, and by the η production threshold at 1489 MeV (for the S_{11} state only). Some of the poles and zeros may be intimately connected with these thresholds.

In Fig. 9 we map $\ln(T^2)$ extended into the complex energy plane to illustrate how prominent features of the on-shell partial waves are influenced by nearby poles and zeros of the T matrix.

Generally there is a close association between the poles of Table V and πN resonances given in the baryon table of the Particle Data Group.[2] Some of the structures, however, are too complicated to be described by simple resonance forms; therefore, we are presently engaged in a more extensive study of the complex-plane topology for solution FP84.

TABLE V. Complex-plane positions for prominent partial-wave poles (P) and zeros (Z). Positions are in c.m. energy (Re W,Im W) MeV. Resonances are from the baryon table (Ref. 2) and indicate their (one—four)-star rating.

State	Resonances	Pole (P), or Zero (Z)
S_{11}	1535****	P_1 (1461, −70)
	1650****	Z_1 (1580, −69)
		P_2 (1660, −61)
P_{11}	1440****	Z_1 (1200,0)
	1710***	P_1 (1359, −100)
		P_2 (1410, −80)
		Z_2 (1880, −70)
P_{13}	1540*	Z_1 (1691, −15)
	1720****	P_1 (1705, −40)
D_{13}	1520****	P_1 (1510, −61)
	1700***	Z_1 (1651, −46)
		P_2 (1670, −40)
		Z_2 (1890, −141)
D_{15}	1675****	P_1 (1661, −71)
F_{15}	1680****	P_1 (1680, −60)
S_{31}	1620****	Z_1 (1585, −34)
		P_1 (1599, −60)
P_{33}	1232****	P_1 (1210, −50)
	1600**	Z_1 (1590, −60)
	1920***	P_2 (1581, −150)
D_{33}	1700****	Z_1 (1360, −21)
		P_1 (1668, −160)
F_{35}	1905****	Z_1 (1557, −52)
		P_1 (1830, −90)
F_{37}	1950****	P_1 (1858, −119)

VIII. COMPARISON WITH KARLSRUHE-HELSINKI SOLUTIONS

In Fig. 7 partial waves through $l=3$ from solution FP84 are plotted with values obtained by the Karlsruhe-Helsinki (KH) group.[1] Comparison reveals good agreement below 600 MeV, and fair agreement above 600 MeV. In particular, FP84 does not contain some of the smaller structures of the KH solution. Some of this can be attributed to the higher degree of smoothing which is intrinsic to our method; comparison with our single-energy analyses, however, suggests that these structures are not being demanded by the data. Some of the structures are possibly noise in the KH solutions.

The principal difference between our method and that of the KH group is in the larger amount of dispersion-theoretic data used by the KH group to constrain their solutions. We use only the real part of the forward amplitude[3] to complement real scattering data. The KH analyses are also much more ambitious, covering an energy range nearly three times that which we cover. Our primary emphasis is the precise encoding of scattering data in our more limited energy range through solutions which have proper direct-channel analytic properties, and which can be analytically extended into the complex energy plane to reveal dominant dynamical features such as poles and zeros of the resultant partial waves. It is encouraging that these two quite different approaches produce such similar results.

IX. THE SAID FACILITY: EXPLORING THE SOLUTIONS

A package of programs and data files known as SAID (scattering analyses interactive dial-in) is used to encode these π-nucleon analyses, including pion-production analyses,[4] as well as recent analyses of nucleon-nucleon and

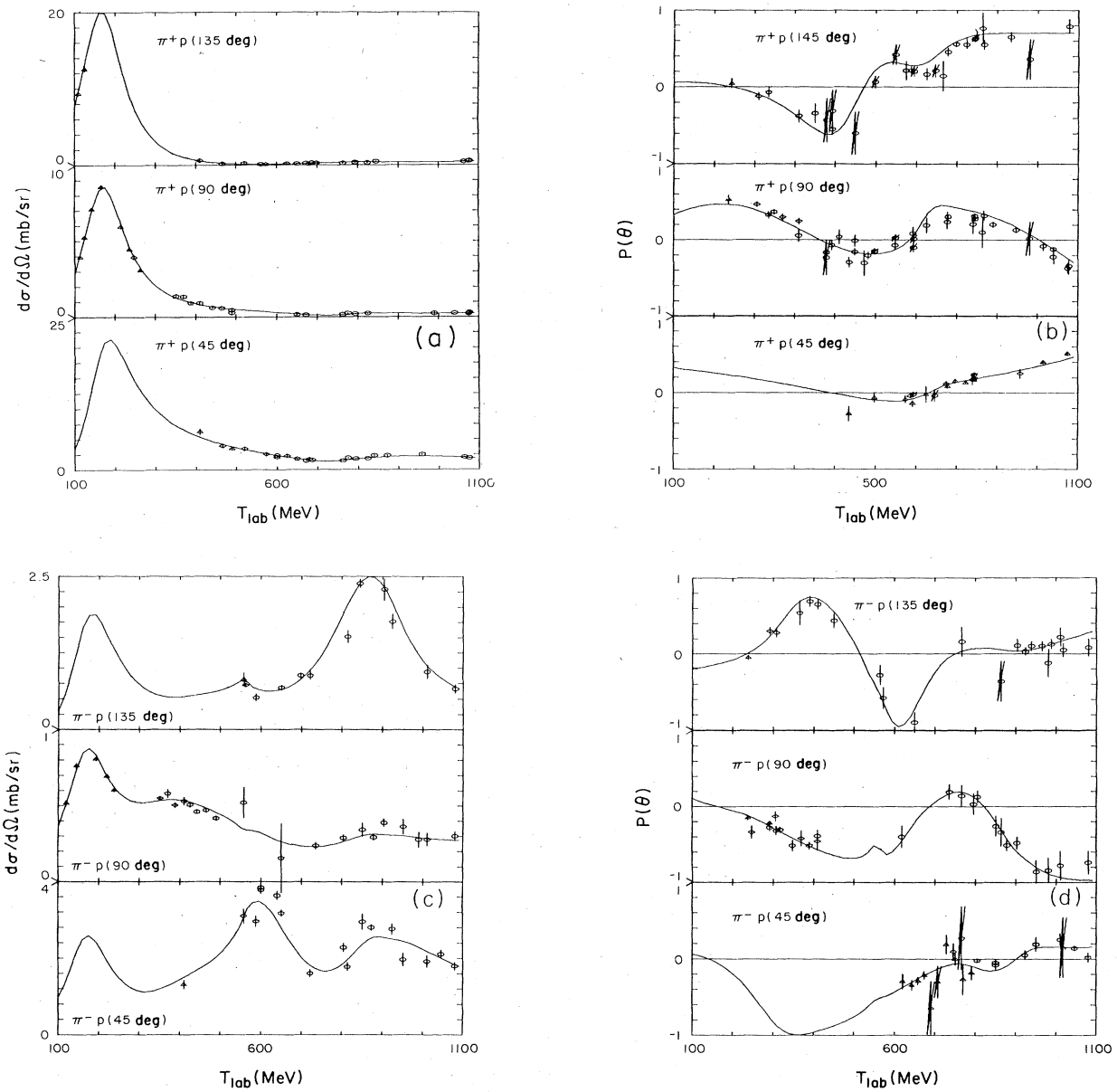

FIG. 8. Our FP84 solution versus some of the angular data. P=polarization, CXS=charge-exchange reaction. The data shown are within $\pm 1°$ of the selected angle. (a) Differential cross sections for π^+p. (b) Polarizations for π^+p. (c) Differential cross sections for π^-p elastic. (d) Polarizations for π^-p elastic. (e) Differential cross sections for π^-p charge exchange. (f) Polarizations for π^-p charge exchange.

K^+-nucleon data below a few GeV. The programs run interactively on computers at VPI&SU and on many VAX11-780/VMS systems throughout the world. The programs allow use of any of many solutions, including ones which may be entered by the user, to calculate any of the multitude of quantities which are predicted by the solution (observables or partial-wave amplitudes). These, in turn, can be used to plan experiments, examine the data base, and ascertain disparities and uncertainties in the solutions. The system can be used with any computer terminal and a number of terminal types are supported for graphics output (including color graphics on the NEC APC). Most of the plots presented in this report were generated through SAID. Copies of SAID are available upon request on small VAX backup tapes.

The SAID package also contains a set of FORTRAN subroutines which use an interpolating array written for SAID to provide a very accurate reconstruction of on-shell amplitudes in calculations. Users who need on-shell πN amplitudes at a number of kinematic points can simply call these subroutines when necessary from their programs. This package (subroutines and interpolating array) can be obtained on computer tape from the authors.

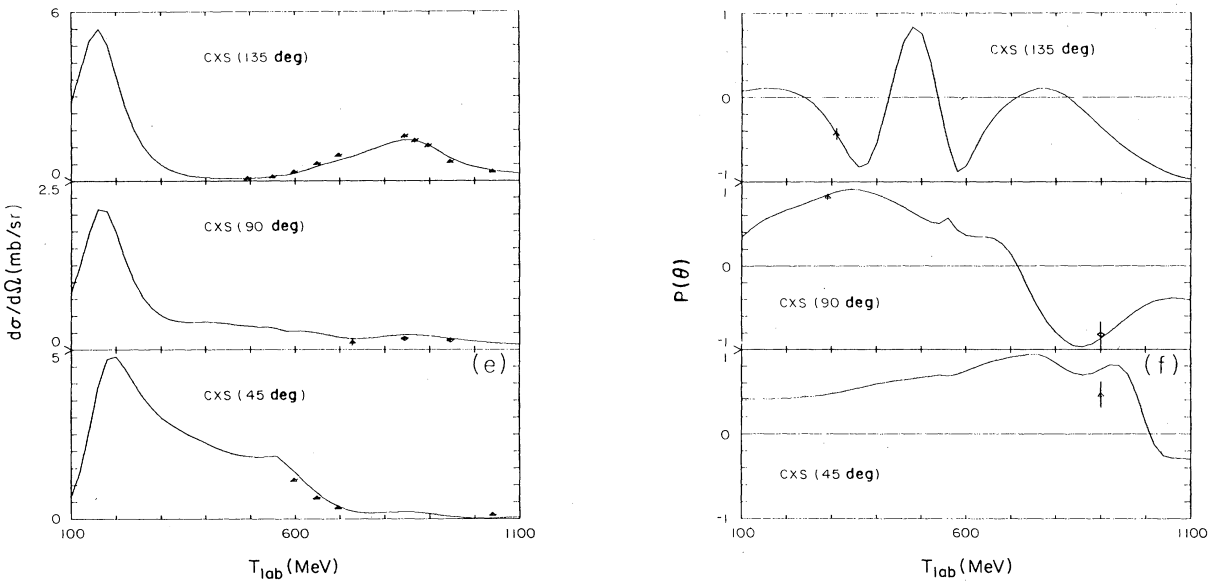

FIG. 8. (*Continued*).

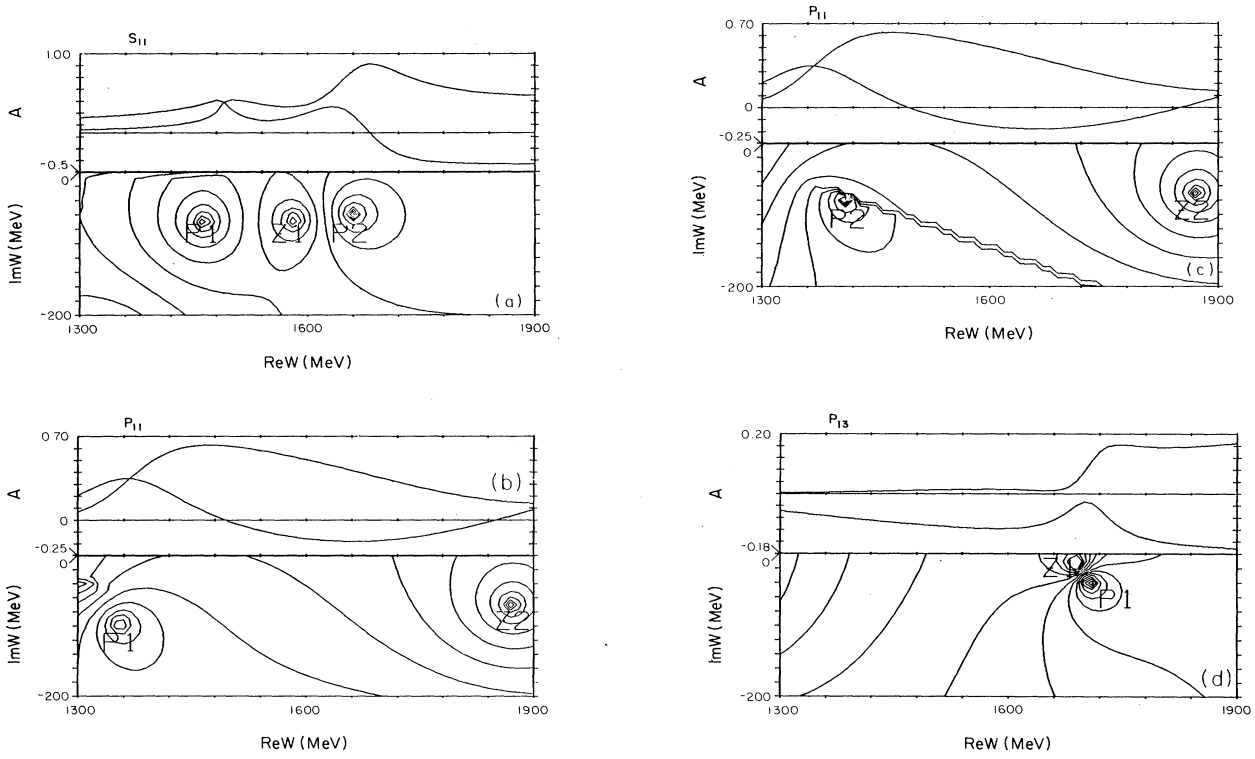

FIG. 9. Complex-plane mapping for selected partial waves. Re W goes from 1300 to 1900 MeV except for P_{33} where it goes from 1100 to 1700 MeV. Im W goes from -200 to 0 MeV (the physical axis). The quantity being mapped is $\ln(T^2)$; prominent poles (P), and zeros (Z) are indicated as described in Sec. VII. The $\pi\Delta$ cut is extended to the left, except for the second view of P_{11} which shows it extending to the right. The partial-wave amplitudes are plotted above the contour plots.

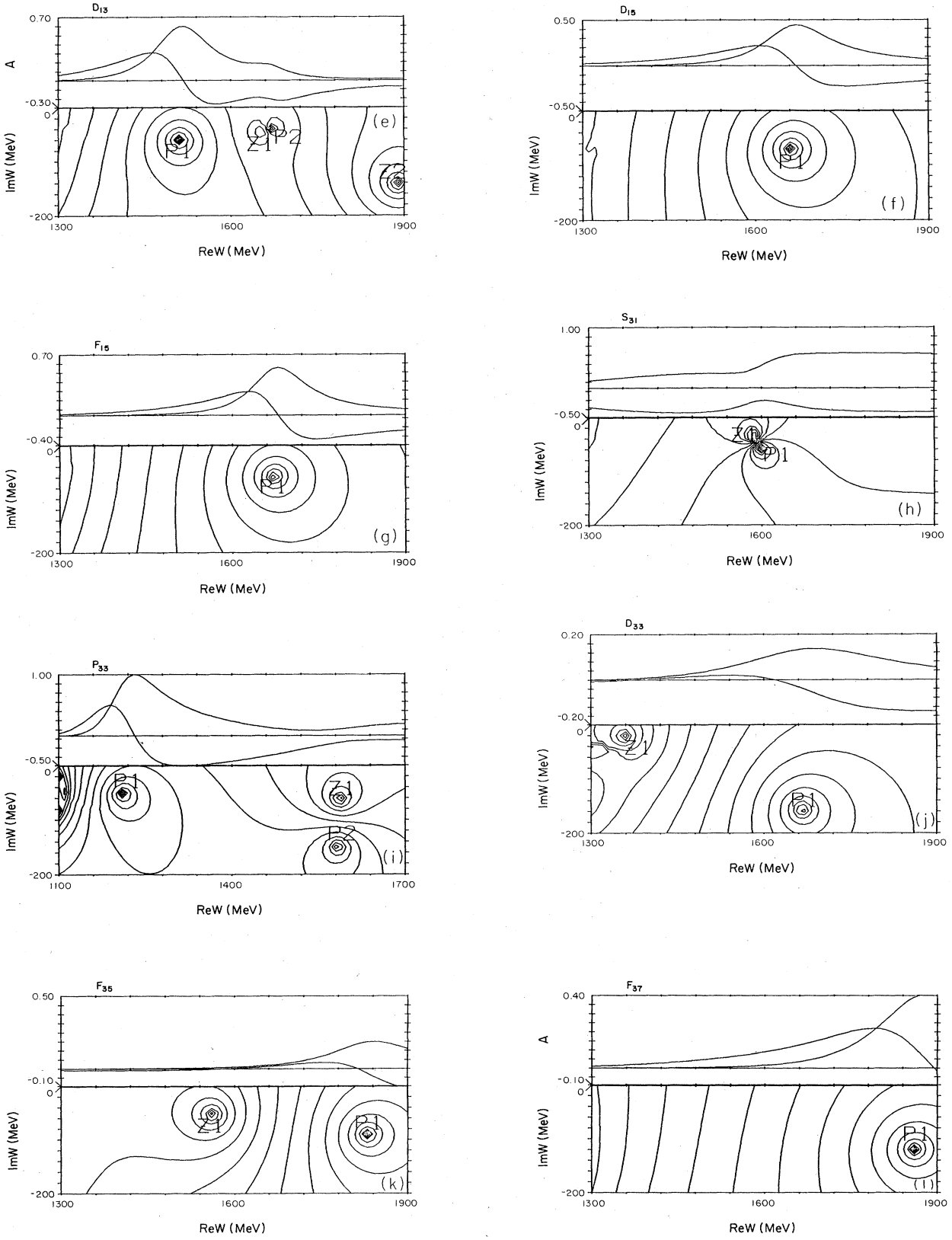

FIG. 9. (*Continued*).

ACKNOWLEDGMENTS

This work was sponsored by the United State Department of Energy under Contract No. DE-AS05-76-ER04928. The authors wish to express their gratitude to Professor B. M. K. Nefkens at UCLA for useful discussions about the data base, and, especially, to Professor G. Höhler at Institüt für Kernphysik (Karlsruhe) for many useful discussions of the data base and several other general aspects of the πN scattering problem. One author (R.A.A.) would like to thank Professor G. Chew at University of California, Berkeley, for the inspiration to present our results in the form of the complex-plane mappings shown in Fig. 9. Another author (J.M.F.) wishes to thank Teledyne Brown Engineering of Huntsville, Alabama, for allowing him leaves of absence to pursue this work.

---

*Permanent address: Brown-Teledyne Engineering, Cummings Research Park, Huntsville, AL 35807.

[1]Karlsruhe-Helsinki (KH) solution: G. Höhler, F. Kaiser, R. Koch, and E. Pietarinen, *Handbook of Pion-Nucleon Scattering* (Fachsinformationszentrum, Karlesruhe, Germany, 1979), Physics Data 12-1; R. Koch, in *Baryon 1980,* proceedings of the 4th International Conference on Baryon Resonances, Toronto, edited by N. Isgur (University of Toronto, Toronto, 1981); R. Koch and E. Pietarinen, Nucl. Phys. **A336**, 331 (1980). The KH solution mentioned in this paper is the high-energy one; the low-energy solution is also available in the SAID facility. Carnegie-Mellon—Berkeley (CMB) solution: R. L. Kelly and R. E. Cutkosky, Phys. Rev. D **20**, 2782 (1979); R. E. Cutkosky *et al., ibid.* **20**, 2804 (1979); **20**, 2839 (1979); R. E. Cutkosky, in *Baryon 1980* (Ref. 1), p. 19.

[2]Particle Data Group, Rev. Mod. Phys. **56**, S1 (1984).

[3]A. A. Carter and J. R. Carter, Rutherford Laboratory Report No. RL-73-024, 1973 (unpublished).

[4]D. Mark Manley, Richard A. Arndt, Yogesh Goradia, and Vigdor Teplitz, Phys. Rev. D **30**, 904 (1984).